Proteomic Profiling and Biological Characterization of Extracellular Vesicles Isolated from Human Alzheimer's Disease Brain Tissues

Satoshi Muraoka[1*], Annina M. DeLeo[1*], Manveen K. Sethi[2*], Kayo Yukawa-Takamatsu[1], Zijian Yang[3], Jina Ko[3], John D. Hogan[4], Sarah A. Daley[5], Zhi Ruan[1], Yang You[1], Yuzhi K. Wang[1], Seiko Ikezu[1], Weiming Xia[1,5], Santi Gorantla[6], Howard E. Gendelman[6], David Issadore[3], Joseph Zaia[2], Tsuneya Ikezu[1,7,8#]

[1]Department of Pharmacology and Experimental Therapeutics, Boston University School of Medicine, Boston, MA 02118, USA, [2]Department of Biochemistry, Boston University School of Medicine, Boston, MA 02118, USA, [3]Department of Bioengineering, University of Pennsylvania, Philadelphia, PA 19104, USA, [4]Program in Bioinformatics, Boston University, Boston, MA 02215, USA, [5]Geriatric Research, Education and Clinical Center, Edith Nourse Rogers Memorial Veterans Hospital, Bedford, MA 01730, USA, [6]Department of Pharmacology and Experimental Neurosciences, University of Nebraska Medical Center, Omaha, NE 68198, USA, [7]Department of Neurology, Boston University School of Medicine, Boston, MA 02118, USA, [8]Center for Systems Neuroscience, Boston University, Boston, MA 2215.
[*]These authors contributed equally to this manuscript

[#]**Correspondence author:** Tsuneya Ikezu, MD, PhD

Boston University School of Medicine, 72 East Concord St, L-606B, Boston, MA 02118,

USA. Email: tikezu@bu.edu Phone: 617-358-9575 Fax: 617-358-9574

Keywords: **Alzheimer's disease, cortical grey matter, extracellular vesicles, microtubule-associated protein tau, amyloid beta** peptide**, proteome, machine learning**

Abstract

Introduction: Extracellular vesicles (EVs) isolated from human biospecimens contains AD pathogenic molecules, such as amyloid-β peptide (Aβ) and tau, may play a role in the spread of disease in human brain. There is no comprehensive characterization of the molecules in human tissue-derived EVs. We therefore examined the protein composition of EVs isolated from the human brain tissue from patients with AD and an age- and sex-matched control group (CTRL).

Methods: EVs were isolated from the cortical grey matter of AD (n=20) and Control (n=18). Tau and Aβ in the EVs were measured by immunoassay. Differentially expressed EV proteins were observed by quantitative proteomics employing machine learning.

Results: The levels of pS396 tau and Aβ were significantly enriched in AD EVs. Proteomic profiling shows enrichment of neuron-specific molecules in control EVs, and glial cell type-specific molecules in AD EVs. Machine learning approach of training group identified annexin A5 (ANXA5), neurosecretory protein VGF, neuronal membrane glycoprotein M6-a (GPM6A), and alpha-centractin (ACTZ) as most distincive molecules in AD EVs compared to the CTRLs. Each of the proteins were confirmed with 88% accuracy in testing group.

Discussion: These data posit that in addition to Aβ and tau, the protein levels of ANXA5, VGF, GPM6A, and ACTZ are significantly altered in AD brain-derived EVs.

1. Background

Alzheimer's disease (AD) is one of the most common forms of dementia, with nearly 50 million individuals worldwide afflicted by the disease. AD is neuropathologically characterized by the presence of amyloid plaques which are formed by extracellular aggregation of amyloid beta peptide (Aβ) and neurofibrillary tangles (NFTs) formed by the accumulation of hyperphosphorylated and misfolded microtuble-associated protein tau in the brain [1,2]. As AD progresses, Aβ and tau aggregates spread through the brain in a characteristic and predictable spatiotemporal manner [3,4]. Aβ deposition are known to occur in the frontal and temporal lobes, hippocampus and limbic system, while NFT deposits appear in medial entorhinal cortex and hippocampus, and progressively spread to other areas of the neocortex [3]. Tau pathology was classified by Braak and Braak as occuring in six histopathological stages corresponding to tauopathy stages of AD. In stages I and II, tau deposits appear into the entorhinal cortex and hippocampus,while in stage III and IV, higher density is present beyond entorhinal cortex and hippocampal regions to neocortical regions. In the final stages, V-VI, pathological tau deposits are present in all components of the hippocampus [3].

Extracellular vesicles (EVs), including exosomes (50-150nm), ectosomes / microvesicles (150-1000nm), and apoptotic bodies (1000-5000nm), are released from neurons, glia, and various other cells into the extracellular space [5-7]. These vesicles contain several forms of nucleic acids (microRNA, ncRNA, mRNA, DNA among others), lipids and proteins that can be transferred to recipient cells as a form of cell-to-cell communication. EVs are found in all body fluids, including blood, urine, and cerebrosprinal fluids (CSF) [8,9]. In the central nervous system (CNS), it has been reported that AD-associated pathogenic molecules, including tau and Aβ, are present in EVs, which may play important roles in AD pathogenesis [9-11]. Recent

research has revealed the presence of Aβ and tau oligomers in neuron and brain-derived EVs [12,13]. Moreover, it has been reported that inhibition of EV synthesis reduced amyloid plaque deposition in the mouse model of AD, and stimulation of EV secretion increased intracellular transfer of prion protein [14,15]. However, the role of EVs in the aggregation or clearance of Aβ remains unclear. EVs are involved in the extracellular enzymatic degradation of Aβ and are shown to promote Aβ aggregation and clearance by microglia [16,17]. On other hand, several researchers have reported the models of neuron-to-neuron transfer of tau seeds by EVs [12,18-20]. Previous work in our lab has shown that microglia spread tau via EV secretion, and that inhibiting EV synthesis significantly reduced tau propagation *in vitro* and *in vivo* [10]. More recently, Bridging integrator 1 (BIN1) is associated with the progression of tau pathology by altering tau clearance and promoting the release of tau-enriched EV by microglia [21]. Previous studies have analyzed and characterized EV isolated from human and mouse brain tissue by morphology, proteomics, and RNA analysis [22-25]. However, no comprehensive and quantitative proteomics database for EVs isolated from the AD and control brain tissues exists. Herein, we provide the first proteomic profiling of EVs isolated from postmortem brain tissues of both AD and cognitively unimpaired cases, which is combined with machine learning. Furthermore, we assessed the amount of Aβ and tau sepeices by specific ELISA. The machine learning approach identified candidate molecules for distinguishing the AD brain-derived EVs and control brain-derived EVs in a high accuracy.

2. Methods

2.1. Sample selection

Two cohorts of brains were used in this study. The first cohort was obtained from the University of Nebraska Medical School (11 AD and 9 CTRL) and the Greater Los Angeles Veteran's Affairs Hospital in association with the University of California, Los Angeles (9 AD and 9 CTRL), which were matched for age and sex. The second cohort was obtained from the NIH neuro-BioBank (22 AD and 18 CTRL) that were age- and sex-matched. The Institutional Review Board at the University of Nebraska Medical School, the University of California, Los Angeles, and the NIH neuro-BioBank approved the protocol, and all participants provided informed consent.

2.2. Purification of EVs from human brain samples

0.5 g of largely grey matter tissue from the frontal cortex of deceased AD or CTRL patients were processed for EV extraction based on reported method with some modifications [23]. Briefly, frozen brain tissue was chopped on ice using a razor blade (# 12-640 Fischer Scientific) to generate 2-3 mm^3 sections. The sections were transferred to 3mL of Hibernate E solution containing 20 units of Papain (# LK003178 Worthington-biochemical corporation) in Earle's Balanced Salt Solution (EBSS) (# 14155063 Gibco) and then incubated in a water bath at 37°C for 15 minutes by stirring once every 5 minutes. After incubation, the samples were immediately place on ice, and 6mL of ice-cold Hibernate E solution (# A1247601 Gibco). The dissociated brain tissue samples were gently homogenized (20 strokes) with a glass-Teflon homogenizer (# 89026-384 VWR). The homogenized tissue samples were filtered with 40 μm mesh filter (# 22-363-547 Fisher scientific). After filtration, the tissue samples were centrifuged at 300g for 10 min at 4°C (# 5720R Eppendorf). The supernatant from 300g was transferred to new 15mL tube and then centrifuged at 2,000g for 10 min at 4°C (# 5720R Eppendorf). The supernatant from 2,000g was transferred to 30mL conical tube and then centrifuged at 10,000g for 10 minutes at

4°C (# Avanti J-E JA25-50 Beckman Coulter). The supernatant from this spin was filtered through a 0.22 μm mesh filter (# SLGP033RS EMD Millipore) into new a polyallomer ultracentrifuge tube with 13.2mL capacity (# 331372 Beckman Coulter) and then was centrifuged at 100,000g for 70 minutes at 4°C (# Optima-XE SW41 Beckman Coulter). After ultracentrifugation, the supernatant was completely discarded, and the pellet was resuspended in 2mL of 0.475M of sucrose solution (# S5-3 Fisher science). All sucrose solutions were diluted in double-filtered PBS (dfPBS) with 0.22 μm pore-size (# SLGP033RS EMD Millipore). The sucrose step gradient was created with six 2-mL steps starting from 2.0 M to 1.5M, 1.0M, 0.825M, 0.65M, and 0.475M (containing the resuspended pellet) in a polyallomer ultracentrifuge tube. Each layer was colored with commercially available food coloring to facilitate capture of the EV-rich interphase present between certain steps. The gradient was centrifuged at 35,000 RPM for 20 h at 4°C (# Optima-XE SW41 Beckman Coulter), after centrifugation, the gradient was collected in 2mL fractions, except for the first and last fractions, which were 1 mL each. Fraction III corresponded to the 1 mL removed from the tube, and particles in this area had a buoyant density of approximately 1.08 g/cm^3. The area between the second (0.65M) and third (0.825M) steps was collected and corresponded to fraction “V”, with a buoyant density of 1.10 - 1.12 g/cm^3, while the interphase between the third and fourth steps corresponded to fraction “VI”, with a buoyant density of 1.12 - 1.15 g/cm^3. The V and VI fractions were then diluted separately to a total volume of 12 mL with dfPBS and centrifuged at 100,000g for 70 min at 4°C (# Optima-XE SW41 Beckman Coulter). Final pellet from each fraction was resuspended in 30 μL of dfPBS. For all biochemical analyses, these fractions were combined such that an equal volume of each fraction (V and VI) was used. For proteomics, an equal amount of total protein from each fraction (V and VI) was used.

2.3. Protein concentration Assessment

The bicinchoninic acid (BCA) assay was used to determine protein concentration for each sample. The Pierce BCA protein assay kit was used (# 23225 Pierce). Due to the limited amount of sample, exosomes were diluted 1:10 before loading into the assay, and a 10:80 ratio of sample to reaction components was used. All assays were allowed to incubate at 60°C for 30 mins before protein concentration was read in a Biotek SynergyMix at 562 nm. For all protein assays, raw readings were adjusted by dilution of the sample for the assay, and then by the final dilution of the sample and starting weight of the material. The average concentration was then taken for fractions V and VI.

2.4. Measurement of total tau (t-tau), phosphorylated tau (pT181 tau, pS199 tau, pS396 tau), amyloid beta (Aβ1-40, Aβ1-42) and Annexin V (ANXA5)

EVs were diluted 1:500 in TET buffer (50 mM Tris HCl pH 7.5, 2 mM EDTA, 1% Triton X-100) supplemented with Pierce HALT inhibitor (# 78425 ThermoFisher) for t-tau and ANXA5 or TENT buffer (50 mM Tris HCl pH 7.5, 2 mM EDTA, 150mM NaCl, 1% Triton X-100) supplemented with phosphatase inhibitors (either addition of 0.5mM PMSF, 10 mM NaF (# S7920 SIGMA), 200 mM glycerol-2-phosphate (# 50020 SIGMA), and 1 mM Na_3VO_4 (# S6508 SIGMA)) or Pierce HALT inhibitor for pT181 tau, pS196 tau, and pS396 tau. Enzyme-linked immunosorbent assays (ELISAs) were performed to assess levels of t-tau, p-tau, and ANXA5. Commercially available kits from Thermofisher (t-tau: # KHB0042, pT181: # KHO0631, pS199: # KHO0631, pS396: # KHO0631, ANXA5: # BMS252) were used according to manufacturer's instructions. For Aβ1-40 and Aβ1-42, the levels were measured using the Single Molecule Counting (SMC®) Immunoassay Technology using commercially available kits from Millipore and Sigma (Aβ1-40: # 03-0145-00, Aβ1-42: # 03-0146-00).

2.5. Nanosight Tracking Analysis (NTA)

All samples were diluted in dfPBS at least 1:1000 or more to get particles within the target reading range for the Nanosight 300 machine (Malvern Panalytical Inc), which is 10-100 particles per frame. Using a syringe pump infusion system (Harvard Laboratories/Malvern), five 60-second videos were taken for each sample at 21°C. Analysis of particle counts was carried out in the Nanosight NTA 3.2 software (Malvern Panalytical Inc) with a detection threshold of 5. Particle counts were normalized for dilution on the machine, dilution of the final pellet, and starting material for exosome extraction. The average count was then taken for fractions V and VI.

2.6. Transmission Electron microscopy (TEM)

The EV isolated from AD or CTRL brain tissue were analyzed by TEM. 5µl of the EV sample was adsorbed for 1 min to a carbon-coated grid (# CF400-CU EMS www.emsdiasum.com) that had been made hydrophilic by a 20-second exposure to a glow discharge (25mA). Excess liquid was removed with a filter paper (# 1 Whatman), the grid was then floated briefly on a drop of water (to wash away phosphate or salt), blotted on a filer paper, and then stained with 0.75% uranyl formate (# 22451 EMS) for 15 seconds. After removing the excess uranyl formate with a filter paper, the grids were examined in a JEOL 1200EX Transmission electron microscope and images were recorded with an AMT 2k CCD camera.

2.7. Mass Spectrometry

2.7.1. Sample Preparation

2,2,2-Trifluoroethanol (TFE) (# 75-89-8 Milipore) was added to the EV samples to a final concentration of 50%. The samples were sonicated for 2 min on an ice-water bath (VWR Scientific) and then incubated at 60°C for 2 h. After cool down, the 5 mM dithiothreitol (# 3483-12-3 Sigma Aldrich) was added to the samples, and then reduced for 30 min at 60°C. Further, the

samples were alkylated with 10 mM iodoacetamide (# 163-2109 BioRad) for 30 min at room temperature in the dark. The samples were digested with mass spectrometry grade trypsin (# V5280 Promega) in 50 mM ammonium bicarbonate (pH 7.5) for protein digestion (1:30 w/w trypsin-to-protein) for 16h at 37°C. The digested peptides were dried by vacuum centrifugation (# SPD1010 Speedvac system, Thermo Savant). The dried samples were resuspended in 2% acetonitrile/water/0.1% trifluoro acetic acid (TFA) and desalted using C-18 spin columns (# 89870 ThermoScientific); the cleaned peptides were eluted using 60% acetonitrile (ACN) /water/0.1% TFA, dried by vacuum centrifugation (# SPD1010 Speedvac system, Thermo Savant) and further resuspended in 1% ACN/water/0.1% formic acid (FA) and analyzed by nano-liquid chromatography and tandem mass-spectrometry (Nano-LC-MS/MS).

2.7.2. Liquid Chromatography (LC)- Electrospray Ionization (ESI) Tandem MS (MS/MS) Analysis

Nano-LC-MS/MS analysis was conducted by an Q-ExactiveHF mass spectrometer (Thermo-Fisher Scientific) equipped with a nano ultra-performance liquid chromatography (UPLC) (Water Technology) Peptides were trapped on a separated on a trapping (180 µm x 20 mm) column and separated on a reversed phased C-18 analytical (BEH C18, 150 µm x 100 mm) column (Waters technology). We loaded 1 µL onto the column and separation was achieved using a 75 min gradient of 2 to 98% ACN in 0.1% FA at a flow rate of ~500 nL/min. Data-dependent acquisition tandem MS was acquired in the positive ionization mode for the top 20 most abundant precursor ions. The scan sequence began with an MS1 spectrum (Orbitrap; resolution 60,000; mass range 300-2000 m/z; automatic gain control (AGC) target 1×10^6; maximum injection time 100 ms). MS2 analysis consisted of higher energy collisional

dissociation (Orbitrap; resolution 15,000; AGC 1×10^5; normalized collision energy (NCE) 30; maximum injection time 100 ms, dynamic exclusion time of 8 s).

2.7.3. Sequence Database Searching and Data Analysis

The raw LC-MS/MS data were converted into mZXML format using ProteoWizard msConvert [26]. The data were searched using PeaksDB and PeaksPTM using Peaks Studio version 8.0 (Bioinformatics Solutions, Inc., Waterloo, ON, Canada) against the Uniprot/Swissprot database for Homo sapiens with a 0.1% false discovery rate (FDR) and at least two unique peptides. A 10-ppm error tolerance for the precursor (MS1) and 0.02 Da mass error tolerance for fragment ions (MS2) were specified. A maximum of 3 missed cleavages per peptide was allowed for the database search, permitting non-tryptic cleavage at one end. Trypsin was specified as the enzyme and carbamidomethylation as a fixed modification. A peaksPTM search was queued after the peaksDB search, using advanced settings of a larger set of variable modifications, including hydroxylation P, oxidation M, hydroxylation K, hydroxylation-Hex K, hydroxylation-Hex-Hex K, HexNAc ST, HexHexNAc ST, phosphorylation STY, ubiquitination K, deamidation N, methoxy K, and nitrotyrosine Y. The final protein list generated was a combination of peaskDB and peaksPTM searches. The label-free quantification was achieved using PEAKS Studio Quantification-label-free module with a setting of mass error tolerance of 10 ppm and a retention time shift tolerance of 2.0 min. For data filtering for label-free peptide quantification following parameters was used: significance 15, fold change 1, quality 0, average area 1E4, charges from 1-10. The protein quantification following settings was used: significance 0, fold change 1, at least 2 unique peptides, significance method PEAKS.

2.8. Statistical Analyses

Statistical analysis was conducted using IBM SPSS software ver.25 and GraphPad Prism6. Between-group comparisons were analyzed by Student's t-test, nonparametric Mann-Whitney U, or one-way ANOVA followed by Bonferroni correction for multiple comparisons. The Gene Ontology of identified proteins were elucidated by DAVID Bioinformatics Resources 6.8. (https://david.ncifcrf.gov). The Venn diagram were generated using Venny_2.1 (http://bioinfogp.cnb.csic.es/tools/venny/).

2.9. Machine Learning

The protein biomarkers to distinguish patients with Alzheimer's from controls were selected using Least Absolute Shrinkage and Selection Operator (LASSO) on the proteomics data from the training set (n = 21), where each patient's true state is labeled. An ensemble machine learning classifier to evaluate the performance of the selected proteins was developed. The ensemble machine learning classifier consists of five individual machine learning algorithms to mitigate overfitting, including Linear Discriminant Anlysis, Logisitic Regression, Naïve Bayes, Support Vector Machine, and K-Nearest-Neighbours. The selected proteins' performance on a separate, user-blinded test set was validated (n = 17).

3. Results

A total of 38 patient samples consisted with 20 AD (15M, 5F, Mean age: 75.0) and 18 CTRL (14M, 4F, Mean age: 75.7) cases were included for biological measurement and proteomics analysis of EVs. A total of 78 patient samples consisted with 42 AD (24M, 17F, Mean age: 81.0) and 36 CTRL (22M, 15F, Mean age: 79.0) cases were included for validation analysis **(Table 1)**. There is statistical difference in the demographics between AD and CTRL group except

postmoterm interval (PMI) of validation set, which will be discussed in the validation study (Figure 4E).

3.1. Experimental workflow

The experimental workflow is summarized in **Figure 1A**. The EVs were isolated from 20 AD and 18 sex- and age-matched cognitively unimpaired controls (CTRL) using the discontinuous sucrose gradient ultracentrifugation as previously described with modifications (see Materials and Methods) [23].

3.2. Biochemical characterization of brain-derived EVs

To determine the purity of our EV preparation, we first used Nanoparticle tracking analysis (NTA), which determines the size of suspended particles based on their Brownian motion. Wetherefore prepared two cohorts of brain EVs (AD and CTRL) and analyzed their size and number by NTA. The concentration of EVs derived from AD and CTRL brains was not significantly different ($p = 0.6075$). The mode size distribution for EVs was significantly different, and peaked at 122 nm for AD and 131 nm for CTRLs ($p = 0.0095$) **(Figure 1B)**. The EVs isolated from frozen brain tissue showed cap-sharped morphology by transmission electron microscopy (TEM) **(Figure 1C)**. To characterize the AD-related proteins carried by brain-derived EVs, we measured the concentration of total tau (t-tau) and phosphorylated tau protein at threonine 181 (pT181 tau), serine 199 (pS199 tau) and serine 396 (pS396 tau) in lysed EVs by specific ELISA. T-tau, pT181 tau, and pS199 tau showed no significant differences between AD and CTRL (t-tau: $p = 0.398$, pT181 tau: $p = 0.7235$, and pS199 tau: $p = 0.4384$) **(Figure 1D)**. Conversely, pS396 tau was significantly increased in AD-brain derived EVs over CTRL (pS396

tau: $p = 0.0375$) **(Figure 1D)**. Moreover, we observed significant increase of both Aβ1-40 and Aβ1-42 in AD-derived EVs over CTRLs (Aβ1-40: $p = 0.0021$ and Aβ1-42: $p < 0.0001$) **(Figure 1E)**.

3.3. Proteomics profiling of EVs isolated from brain tissues

We performed non-label Nano-LC-MS/MS analysis of 38 EV samples for proteomic profiling. Across both cohorts, a total of 1,088 proteins were identified with at least two unique peptides **(Figure 2A and Supplementary Table 1 and 2)**. There were 940 proteins identified in CTRL EVs and 1,000 proteins identified in AD EVs. Among them, 852 proteins were detected in both groups, with 88 proteins unique to the CTRL and 148 proteins unique to the AD group **(Figure 2A)**. The common, AD unique and CTRL unique proteins were tested for properties pertaining to the 'cellular component' and 'pathway' ontologies by Gene Ontology analysis in the Database for Annotation, Visualization and Integrated Discovery (DAVID). Among the 852 shared proteins, 60.9% were found to be included in the extracellular exosome ontology **(Figure 2B)**. The 148 proteins unique to the AD group were involved in mitochondria metabolism, which likely reflects the mitochondrial dysfunction known to occur in AD brain [27] **(Figure 2B)**. Interestingly, in pathway analysis by DAVID, neurodegenerative disease, including Alzheimer's, Parkinson's, and Huntington's disease were enriched in common proteins, as well as those proteins unique to the AD group **(Figure 2C). Figure 2D** shows the peptides identified by Nano-LC-MS/MS, which covered 55.1% of Tau (1-441), 9.1% of amyloid-beta precursor protein (APP 1-770), 74.3% of alpha-synuclein (SNCA 1-140), and 6.3% of apolipoprotein E (APOE 1-317). Posttranslation modification (PTM) analysis detected six phosphorylation sites (pT181, pS198, pS199, pS202, pT231, and pS404) on tau protein **(Figure 2D,** red bold letters**)**. Notably, Aβ

peptides sequence was identified in APP. **Figure 2E** shows AD pathway from KEGG pathway analysis based on 68 proteins identified in the AD group, which are designated with red stars. The list of AD pathway-related proteins are provided in **Supplementary Table 3**. Proteins known to play an important role in AD pathogenesis, such as APP, APOE, tau, NADH-ubiquinone oxidoreductase (Cx I-V), were all identified in the AD group, although they were not unique to this group.

3.4. Analysis of label-free quantitative proteomics comparison of AD brain-derived EV and CTRL brain-derived EVs

Label-free quantitative proteomics analysis was performed using PEAKS studio software. A total of 949 proteins were quantified **(Figure 3A, Supplementary Table 4)**. The 934 quantified proteins were common between AD and CTRL groups. Between these groups, 3 proteins were uniquely expressed in the CTRL group, while 12 proteins were uniquely expressed in the AD group. The principal component analysis (PCA) showed a marginal separation of the two groups **(Figure 3B)**. **Figure 3C** shows the volcano plot of the common 289 proteins which were detected in more than 50% of the group (AD: $n > 10$ and CTRL: $n > 9$). Among these proteins, 15 proteins were significantly up-regulated and 3 proteins were significantly down-regulated in AD compared to the CTRL group as determined by $p < 0.05$ and log2 fold change threshold of >1 or <-1) **(Figure 3C, and Table 2)**. The expression levels of identified 18 molecules in AD group relative to CTRL group are displayed in a heatmap **(Figure 3D)**. We next searched for brain cell-type specific molecules within the EV proteomics dataset using the mouse proteomics dataset as reference [28]. Top 100 ranked cell type-specific molecules, which have at least 5-fold change in concentration in the cell type of interest over the other cell types, were tested with our EV

proteomics dataset **(Figure 3E)**. The distribution of these markers indicate that in the human brain, neuron-derived EV represent 49% of EVs, while the other 50% of EVs are derived from glial cell types, including microglia, astrocytes and oligodendrocytes. Moreover, using label-free quantitative value, we investigated differences in the expression of cell type-specific marker molecules between AD and CTRL groups **(Figure 3F)**. Interestingly, neuron-specific molecules were enriched in the CTRL group (Figure 3F, blue), while glia-specific marker molecules were enriched in the AD group (Figure 3F, red). These results suggested that glia enhances their contribution to generate EVs in AD brains, which may play a role for spreading AD pathology.

3.5. Machine learning model to identify AD brain-specific EV biomarker molecules

To discover the optimal combination of protein biomarkers that distinguish AD from CTRLs, the label-free quantitative proteomics dataset was analyzed using machine learning method **(Figure 4A).** For this purpose, we split the proteomics dataset into unblinded training subset (AD: n = 11; CTRL: n = 10) and blinded testing subset (AD: n = 9; CTRL: n = 8). The decision trees were built using only the data from the training subset, and then the accuracy of the diagnosis was determinedusing the blinded testing set. We found that a panel that included annexin-A5 (ANXA5), NGF-induced growth factor (VGF), neuronal membrane glycoprotein M6-a (GPM6A), and alpha-centractin (ACTZ), using the Lasso algorithm resulted in an area under the ROC curve (AUC) of 0.95 (**Figure 4B** and **Supplementary Table 5).** We then examined the accuracy in the independent blinded test set using the 4 proteins in the dotted green box **(Figure 4B)**. Testing analysis revealed 88% accuracy (AUC = 0.97) in identifying AD patients using ANXA5, VGF, GPM6A, and ACTZ **(Figure 4C).** Further, we ran two control experiments that randomly selected 4 proteins from a total possible 946 proteins to form the diagnosis panel

(repeated 20 times, AUC = 0.58, Accuracy = 55%) and shuffling the true labels of the subjects within the training set (AUC = 0.47, Accuracy = 48%). The control's AUC was significantly worse than using the 4-protein panel's AUC (P<0.001) **(Figure 4C)**. **Figure 4D** shows the scatter plot of selected 4 proteins, which were significantly different between AD and CTRL groups **(Supplementary Table 6)**. Next, we assessed the correlation of expression of these candidate molecules and levels of phosphorylated tau (p-tau), Aβ1–40 and Aβ1–42 in EVs by Pearson's correlation analysis. There was a significantly positive correlation between GPM6A and pS396 tau, and of GPM6A and Aβ1-42 levels (pS396 tau: r = 0.380, p = 0.019; Aβ1-42: r = 0.387, p = 0.016), and a significantly negative correlation between VGF and Aβ1-42 levels (r = -0.538, p = 0.002) **(Figure 4E)**. We also exmined the fist and second cohorts of AD and CTRL cases to validate ANXA5 expression level by ELISA. ANXA5 expression level was significantly increased in AD brain-derived EV compared to the CTRL group (p = 0.0042, 42 AD and 36 CTRL cases, **Figure 4F**). Although there was statistical difference in PMI between AD and CTRL cases in the validation cohort (**Table 1**), Pearson's correlation analysis of PMI and ANXA5 levels show no signifanct correlation (r = -0.165, p = 0.149). Thus, this is not due to the diffence in PMI between the two groups. Interestingly, ANXA5 expression level shows a tendency to increase with Braak stages in an AD-dependent manner **(Figure 4F)**. Therefore, ANXA5 is a potential EV biomarker candidate molecule for not only distinguishing AD and CTRL EVs but also as a surrogate marker for the Braak stage.

4. Discussion

In this study, we provide biophysical properties of EVs isolated from unfixed postmortem human brain tissues, quantitative analysis of tau and Aβ species, and label-free quantitative proteomic

profiling by Nano-LC-MS/MS analysis. We found that pS396 tau, Aβ1-40, and Aβ1-42 levels were significantly increased in AD brain-derived EVs compared to CTRL group. We identified 1,088 unique proteins from brain-derived EVs, which were significantly enriched for the extracellular exosome molecules and the AD pathway by DAVID Gene Ontology analysis. We also quantified 949 proteins by label-free quantitative proteomics analysis, which were enriched in neuron-specific molecules in CTRL group and glial cell type-specific molecules in AD group. Differentially expressed EV proteins in AD and CTRL brain samples included ANXA5, VGF, GPM6A, and ACTZ as determined by machine learning approach. Using the validation cohort with larger sample size, the increased protein level of ANXA5 in AD group compared CTRL group was confirmed by specific ELISA.

When characterizing brain-derived EVs isolated from AD and CTRL by tau-specific ELISA, the pS396 tau levels is significantly increased in the AD group compared to CTRL group. Previous reports indicate pT181 tau to be an early PTM associated with the AD, while pS199 tau is thought to promote tau accumulation and pS396 tau is associated with tau seeding activity and aggregation [29,30]. The enrichment of pS396 in EVs derived from AD brain tissue might promote the of spread and aggregation of tau in the AD brain. We also observed tau fragments (156-406) in the mid region, which is inclusive of proline-rich domains (151-240), microtuble binding repeat domains (244-369). Tau can be cleaved by various proteases including calpain-1 and 2 (at R230), thrombin, cathepsins, asparagine endopeptidase (at D255, N368), and caspase-2 (at D314) and -3 (at D421) [31-34]. However, many tau fragments identified in AD patients have not been well characterized, and the protease responsible for their generation have not all been identified. In cerebrospinal fluid (CSF), 25-35 kDa fragment tau has been used as an early marker of AD; however, the protease responsible for this cleavage event is unknown

[35,36]. Further detailed investigation is needed to determine if tau is truncated by proteases and modified by kinases, and are enriched in AD brain-derived EV.

In the present study, we observed that the size of EVs derived from the AD brainsamples was smaller than control brain-derived EV. We propose two possible factors for this finding. First, cholesterol level might be related to EV size; the CNS is known to contain 25% of the body's cholesterol and accumulation of cholesterol is reported to be associated with AD [37]. High cholesterol levels increase Aβ in cellular and animal models of AD, and the chemical that inhibits cholesterol synthesis reduces Aβ in this model [37-41]. Moreover, it has been reported that small EVs contain significantly higher cholesterol than do large EVs [38,39]. Therefore, AD brain cells that accumulate high cholesterol might secrete smaller EVs than controls. The second possibility is that cell of origin determines EV size. Our study found that the human brain-derived EVs were enriched in cell-type specific molecules corresponding to 50% neuronal and 50% glial cell origins. Moreover, the AD brain-derived EVs were enriched with more glial-specific molecules compared to the CTRL EVs. Thus, there is the possibility that the difference in EV size between AD and CTRL groups is due to an increase in smaller, glia-produced EVs among AD patients.

Herein, we report for the first time, the quantitative proteomic analysis of a large-scale brain-derived EV samples isolated from AD and Control patients. 59.5 % of the identified 1,088 proteins were identified as part of the extracellular exosome ontology, and similar enrichment rate of EV-specific molecules was previously reported [22]. Interestingly, in AD brain-derived EVs, glia-specific marker molecules were enriched, while neuron-specific molecules were enriched in CTRLs. Thus, there is a possibility that glia derived EVs play a role as a vehicle to

transfer pathogenic proteins into neurons in AD brains, that are then spreading and propagating tau throughout the brain.

In summary, we have quantified tau and Aβ levels and investigated proteomic profiles in brain-derived EVs from AD, enriched glia cell type-specific molecule in AD brain-derived EVs, and identified ANXA5, VGF, GPM6A, and ACTZ as potential candidate biomarkers for monitoring progression of AD. Zhang et al., has recently reported that *ANXA5* is associated with familial late-onset AD by GWAS [42]. Further, Sohma et al., has reported significantly higher plasma level of ANXA5 in AD patients than in control groups [43]. A number of previous studies in CSF and brain tissue have reported markedly lowered concentration of VGF in AD patients groups compared to cotrols [44-47] . GPM6A expression level has been shown to be downregulated in the hippocampus of AD in transgenic mice [48,49]. It has been reported that GPM6A with palmitoylation is involved in the clustering of lipid rafts, which are themselves enriched in sphingolipids and cholesterol [50]. Thus, GPM6A might be loaded into EVs with high cholesterol levels in AD. In our study, ANXA5 was detected in brain-derived EVs from one brain tissue cohort by commercial ELISA assay, but VGF, GPM6A, and ACTZ were undetectable. Thus, more high sensitivity detection assays are in need for the quantification of these molecules. Finally, the combination of cell type-specific molecules from brain cells, including ANAX5, VGF, GPM6A, or ACTZ, as observed by our study, may serve as potential biomarker candidate molecules in AD patient blood samples.

Acknowledgments

The author thank M. Ericsson (Electron Microscopy Facility, Harvard Medical School) for electron microscopic imaging services.

Funding: This work is in part funded by Alzheimer's Association AARF-9550302678 (AMD & SM), DVT-14-320835 (TI), BrightFocus Foundation (A2016551S), Cure Alzheimer's Fund (TI), NIH RF1AG054199 (TI), NIH R56AG057469 (TI), NIH R01AG054672 (TI), NIH R21NS104609.

Conflicts of Interest: The authors declare that the research was conducted in the absence of any commercial or financial relationships that could be construed as a potential conflict of interest.

Author Contributions: S.M., A.M.D., and T.I. designed research; S.M., A.M.D., M.K.S., K.Y-T., S.A.D., Z.R., Y.Y., and Y.K.W. performed research; S.M., A.M.D., M.K.S., Z.Y., J.K., J.D.H., W.X., J.Z., and T.I. analyzed data; S.G., and H.E.G. provided brain samples; S.M., and T.I. wrote the paper; S.M., A.M.D., M.K.S., S.I., D.I., J.Z., and T.I. edited the paper.

Supplementary Data

The Supplementary data related to this article can be found at:

References

[1] Goedert M, Wischik CM, Crowther RA, Walker JE, Klug A. Cloning and sequencing of the cDNA encoding a core protein of the paired helical filament of Alzheimer disease: identification as the microtubule-associated protein tau. Pnas 1988;85:4051–5. doi:10.1073/pnas.85.11.4051.

[2] Masters CL, Bateman R, Blennow K, Rowe CC, Sperling RA, Cummings JL. Alzheimer's disease. Nat Rev Dis Primers 2015;1:15056. doi:10.1038/nrdp.2015.56.

[3] Braak H, Braak E. Neuropathological stageing of Alzheimer-related changes. Acta Neuropathologica 1991;82:239–59. doi:10.1007/BF00308809.

[4] Thal DR, Rüb U, Orantes M, Braak H. Phases of A beta-deposition in the human brain and its relevance for the development of AD. Neurology 2002;58:1791–800. doi:10.1212/wnl.58.12.1791.

[5] Thery C, Witwer KW, Aikawa E, Alcaraz MJ, Anderson JD, Andriantsitohaina R, et al. Minimal information for studies of extracellular vesicles 2018 (MISEV2018): a position statement of the International Society for Extracellular Vesicles and update of the MISEV2014 guidelines. J Extracell Vesicles 2018;7:1535750. doi:10.1080/20013078.2018.1535750.

[6] You Y, Ikezu T. Emerging roles of extracellular vesicles in neurodegenerative disorders. Neurobiol Dis 2019;130:104512. doi:10.1016/j.nbd.2019.104512.

[7] Delpech J-C, Herron S, Botros MB, Ikezu T. Neuroimmune Crosstalk through Extracellular Vesicles in Health and Disease. Trends in Neurosciences 2019;42:361–72. doi:10.1016/j.tins.2019.02.007.

[8] Becker A, Thakur BK, Weiss JM, Kim HS, Peinado H, Lyden D. Extracellular Vesicles in Cancer: Cell-to-Cell Mediators of Metastasis. Cancer Cell 2016;30:836–48. doi:10.1016/j.ccell.2016.10.009.

[9] DeLeo AM, Ikezu T. Extracellular Vesicle Biology in Alzheimer's Disease and Related Tauopathy. J Neuroimmune Pharmacol 2018;13:292–308. doi:10.1007/s11481-017-9768-z.

[10] Asai H, Ikezu S, Tsunoda S, Medalla M, Luebke J, Haydar T, et al. Depletion of microglia and inhibition of exosome synthesis halt tau propagation. Nat Neurosci 2015;18:1584–93. doi:10.1038/nn.4132.

[11] Rajendran L, Honsho M, Zahn TR, Keller P, Geiger KD, Verkade P, et al. Alzheimer's disease beta-amyloid peptides are released in association with exosomes. Proc Natl Acad Sci USa 2006;103:11172–7. doi:10.1073/pnas.0603838103.

[12] Wang Y, Balaji V, Kaniyappan S, Krüger L, Irsen S, Tepper K, et al. The release and trans-synaptic transmission of Tau via exosomes. Mol Neurodegener 2017;12:5. doi:10.1186/s13024-016-0143-y.

[13] Sardar Sinha M, Ansell-Schultz A, Civitelli L, Hildesjö C, Larsson M, Lannfelt L, et al. Alzheimer's disease pathology propagation by exosomes containing toxic amyloid-beta oligomers. Acta Neuropathologica 2018;136:41–56. doi:10.1007/s00401-018-1868-1.

[14] Guo BB, Bellingham SA, Hill AF. Stimulating the Release of Exosomes Increases the Intercellular Transfer of Prions. J Biol Chem 2016;291:5128–37. doi:10.1074/jbc.M115.684258.

[15] Dinkins MB, Dasgupta S, Wang G, Zhu G, Bieberich E. Exosome reduction in vivo is associated with lower amyloid plaque load in the 5XFAD mouse model of Alzheimer's disease. Neurobiol Aging 2014;35:1792–800. doi:10.1016/j.neurobiolaging.2014.02.012.

[16] Bulloj A, Leal MC, Xu H, Castaño EM, Morelli L. Insulin-degrading enzyme sorting in exosomes: a secretory pathway for a key brain amyloid-beta degrading protease. J Alzheimers Dis 2010;19:79–95. doi:10.3233/JAD-2010-1206.

[17] Yuyama K, Sun H, Mitsutake S, Igarashi Y. Sphingolipid-modulated exosome secretion promotes clearance of amyloid-β by microglia. J Biol Chem 2012;287:10977–89. doi:10.1074/jbc.M111.324616.

[18] Dujardin S, Bégard S, Caillierez R, Lachaud C, Delattre L, Carrier S, et al. Ectosomes: a new mechanism for non-exosomal secretion of tau protein. PLoS ONE 2014;9:e100760. doi:10.1371/journal.pone.0100760.

[19] Polanco JC, Li C, Durisic N, Sullivan R, Götz J. Exosomes taken up by neurons hijack the endosomal pathway to spread to interconnected neurons. Acta Neuropathol Commun 2018;6:10. doi:10.1186/s40478-018-0514-4.

[20] Polanco JC, Scicluna BJ, Hill AF, Götz J. Extracellular Vesicles Isolated from the Brains of rTg4510 Mice Seed Tau Protein Aggregation in a Threshold-dependent Manner. J Biol Chem 2016;291:12445–66. doi:10.1074/jbc.M115.709485.

[21] Crotti A, Sait HR, McAvoy KM, Estrada K, Ergun A, Szak S, et al. BIN1 favors the spreading of Tau via extracellular vesicles. Sci Rep 2019;9:9477. doi:10.1038/s41598-019-45676-0.

[22] Vella LJ, Scicluna BJ, Cheng L, Bawden EG, Masters CL, Ang C-S, et al. A rigorous method to enrich for exosomes from brain tissue. J Extracell Vesicles 2017;6:1348885. doi:10.1080/20013078.2017.1348885.

[23] Perez-Gonzalez R, Gauthier SA, Kumar A, Levy E. The exosome secretory pathway transports amyloid precursor protein carboxyl-terminal fragments from the cell into the brain extracellular space. J Biol Chem 2012;287:43108–15. doi:10.1074/jbc.M112.404467.

[24] Hurwitz SN, Sun L, Cole KY, Ford CR, Olcese JM, Meckes DG. An optimized method for enrichment of whole brain-derived extracellular vesicles reveals insight into neurodegenerative processes in a mouse model of Alzheimer's disease. J Neurosci Methods 2018;307:210–20. doi:10.1016/j.jneumeth.2018.05.022.

[25] Gallart-Palau X, Serra A, Sze SK. Enrichment of extracellular vesicles from tissues of the central nervous system by PROSPR. Mol Neurodegener 2016;11:41. doi:10.1186/s13024-016-0108-1.

[26] Adusumilli R, Mallick P. Data Conversion with ProteoWizard msConvert. Methods Mol Biol 2017;1550:339–68. doi:10.1007/978-1-4939-6747-6_23.

[27] Saman S, Lee NCY, Inoyo I, Jin J, Li Z, Doyle T, et al. Proteins recruited to exosomes by tau overexpression implicate novel cellular mechanisms linking tau secretion with Alzheimer's disease. J Alzheimers Dis 2014;40 Suppl 1:S47–70. doi:10.3233/JAD-132135.

[28] Sharma K, Schmitt S, Bergner CG, Tyanova S, Kannaiyan N, Manrique-Hoyos N, et al. Cell type- and brain region-resolved mouse brain proteome. Nat Neurosci 2015;18:1819–31. doi:10.1038/nn.4160.

[29] Hanger DP, Anderton BH, Noble W. Tau phosphorylation: the therapeutic challenge for neurodegenerative disease. Trends Mol Med 2009;15:112–9. doi:10.1016/j.molmed.2009.01.003.

[30] Takeda S, Wegmann S, Cho H, DeVos SL, Commins C, Roe AD, et al. Neuronal uptake and propagation of a rare phosphorylated high-molecular-weight tau derived from Alzheimer's disease brain. Nat Commun 2015;6:8490. doi:10.1038/ncomms9490.

[31] Rissman RA, Poon WW, Blurton-Jones M, Oddo S, Torp R, Vitek MP, et al. Caspase-cleavage of tau is an early event in Alzheimer disease tangle pathology. J Clin Invest 2004;114:121–30. doi:10.1172/JCI20640.

[32] Zhang Z, Song M, Liu X, Kang SS, Kwon I-S, Duong DM, et al. Cleavage of tau by asparagine endopeptidase mediates the neurofibrillary pathology in Alzheimer's disease. Nat Med 2014;20:1254–62. doi:10.1038/nm.3700.

[33] Kurbatskaya K, Phillips EC, Croft CL, Dentoni G, Hughes MM, Wade MA, et al. Upregulation of calpain activity precedes tau phosphorylation and loss of synaptic proteins in Alzheimer's disease brain. Acta Neuropathol Commun 2016;4:34. doi:10.1186/s40478-016-0299-2.

[34] Zhao X, Kotilinek LA, Smith B, Hlynialuk C, Zahs K, Ramsden M, et al. Caspase-2 cleavage of tau reversibly impairs memory. Nat Med 2016;22:1268–76. doi:10.1038/nm.4199.

[35] Johnson GV, Seubert P, Cox TM, Motter R, Brown JP, Galasko D. The tau protein in human cerebrospinal fluid in Alzheimer's disease consists of proteolytically derived fragments. J Neurochem 1997;68:430–3. doi:10.1046/j.1471-4159.1997.68010430.x.

[36] Portelius E, Hansson SF, Tran AJ, Zetterberg H, Grognet P, Vanmechelen E, et al. Characterization of tau in cerebrospinal fluid using mass spectrometry. J Proteome Res 2008;7:2114–20. doi:10.1021/pr7008669.

[37] Torres M, Busquets X, Escribá PV. Brain Lipids in the Pathophysiology and Treatment of Alzheimer’s Disease. Update on Dementia, InTech; 2016. doi:10.5772/64757.

[38] Durcin M, Fleury A, Taillebois E, Hilairet G, Krupova Z, Henry C, et al. Characterisation of adipocyte-derived extracellular vesicle subtypes identifies distinct

protein and lipid signatures for large and small extracellular vesicles. J Extracell Vesicles 2017;6:1305677. doi:10.1080/20013078.2017.1305677.

[39] Pfrieger FW, Vitale N. Cholesterol and the journey of extracellular vesicles. J Lipid Res 2018;59:2255–61. doi:10.1194/jlr.R084210.

[40] Puglielli L, Tanzi RE, Kovacs DM. Alzheimer's disease: the cholesterol connection. Nat Neurosci 2003;6:345–51. doi:10.1038/nn0403-345.

[41] Evangelisti E, Cecchi C, Cascella R, Sgromo C, Becatti M, Dobson CM, et al. Membrane lipid composition and its physicochemical properties define cell vulnerability to aberrant protein oligomers. Journal of Cell Science 2012;125:2416–27. doi:10.1242/jcs.098434.

[42] Zhang X, Zhu C, Beecham G, Vardarajan BN, Ma Y, Lancour D, et al. A rare missense variant of CASP7 is associated with familial late-onset Alzheimer's disease. Alzheimers Dement 2019;15:441–52. doi:10.1016/j.jalz.2018.10.005.

[43] Sohma H, Imai S-I, Takei N, Honda H, Matsumoto K, Utsumi K, et al. Evaluation of annexin A5 as a biomarker for Alzheimer's disease and dementia with lewy bodies. Front Aging Neurosci 2013;5:15. doi:10.3389/fnagi.2013.00015.

[44] Cocco C, D'Amato F, Noli B, Ledda A, Brancia C, Bongioanni P, et al. Distribution of VGF peptides in the human cortex and their selective changes in Parkinson“s and Alzheimer”s diseases. J Anat 2010;217:683–93. doi:10.1111/j.1469-7580.2010.01309.x.

[45] Llano DA, Devanarayan P, Devanarayan V, Alzheimer’s Disease Neuroimaging Initiative (ADNI). VGF in Cerebrospinal Fluid Combined With Conventional Biomarkers Enhances Prediction of Conversion From MCI to AD. Alzheimer Dis Assoc Disord 2019;Publish Ahead of Print:1. doi:10.1097/WAD.0000000000000328.

[46] Hölttä M, Minthon L, Hansson O, Holmén-Larsson J, Pike I, Ward M, et al. An integrated workflow for multiplex CSF proteomics and peptidomics-identification of candidate cerebrospinal fluid biomarkers of Alzheimer's disease. J Proteome Res 2015;14:654–63. doi:10.1021/pr501076j.

[47] Brinkmalm G, Sjödin S, Simonsen AH, Hasselbalch SG, Zetterberg H, Brinkmalm A, et al. A Parallel Reaction Monitoring Mass Spectrometric Method for Analysis of Potential CSF Biomarkers for Alzheimer's Disease. Proteomics Clin Appl 2018;12:1700131. doi:10.1002/prca.201700131.

[48] Xu P-T, Li Y-J, Qin X-J, Scherzer CR, Xu H, Schmechel DE, et al. Differences in apolipoprotein E3/3 and E4/4 allele-specific gene expression in hippocampus in Alzheimer disease. Neurobiol Dis 2006;21:256–75. doi:10.1016/j.nbd.2005.07.004.

[49] Woo J-M, Park SJ, Kang HI, Kim BG, Shim SB, Jee SW, et al. Characterization of changes in global gene expression in the brain of neuron-specific enolase/human Tau23 transgenic mice in response to overexpression of Tau protein. International Journal of Molecular Medicine 2010;25:667–75. doi:10.3892/ijmm_00000390.

[50] Ito Y, Honda A, Igarashi M. Glycoprotein M6a as a signaling transducer in neuronal lipid rafts. Neuroscience Research 2018;128:19–24. doi:10.1016/j.neures.2017.11.002.

Figure legends

Figure 1. Biophysical and biochemical characterization of EVs isolated from AD and Control brain tissues:

A) Schematic of extracellular vesicle isolation protocol from human frozen brain tissue. Frozen human gray matter cortex was chopped with a razor blade on ice to generate 2-3mm^3 sections.

The cut sections are dissociated in papain in Hibernate-E at 37°C for 15min. The tissue was homogenized with glass-Teflon homogenizer. After differential centrifugation, the EVs were purified by Sucrose step gradient Ultracentrifugation for 20 hours and then resuspended in double-filtered PBS. **B)** Left: Particle numbers of brain-derived EV fraction from CTRL or AD by Nanoparticle tracking analysis. AD-brain derived EVs had no difference in number when adjusted for starting material than CTRL EVs ($p = 0.6075$ by Mann-Whitney test). Right: Particle size of brain-derived EV fraction. Average mode for particle size was smaller in AD brain compared with non-demented control brains ($p = 0.0095$ by Mann-Whitney test). **C)** Cryo-TEM image of frozen human brain-derived EVs. EVs purified from AD, or non-demented CTRL brains were resuspended in double-filtered PBS and loaded onto formvar/carbon-coated copper mesh grids. The grids were then rinsed three times and negatively stained with 0.75% uranyl acetate. Scale bar is 100 nm. Left: CTRL, Right: AD. **D)** Comparison of total tau and tau phosphorylated at threonine 181, serine 199, and serine 396 in EVs. Tau is thought to be a major pathological factor in AD, especially phosphorylated, misfolded, and oligomerized tau. ELISA revealed that there is no difference in total tau to total protein ($p = 0.398$ by Mann-Whitney test). There was no difference in Tau phosphorylated at threonine181 to total tau ($p = 0.7235$) and at serine 199 to total tau ($p = 0.4384$). Tau phosphorylated at serine 396 to total tau was significantly different ($p = 0.0375$). **E)** Comparison of Amyloid beta 1-40 or 1-42 in EVs. ELISA revealed that there is a significant difference in amyloid beta 1-40 or 1-42 to total protein ($p = 0.0259$, $p < 0.0001$ by Mann-Whitney test).

Figure 2. Proteomics profiling of EVs isolated from AD and CTRL brains:

A) Venn diagram representing the number of EV proteins differentially identified in CTRL and AD. **B)** Gene Ontology (GO) analysis using DAVID Bioinformatics Resources 6.8. The GO term of Top5 Cellular Component with -log10 (FDR *p*-value). **(C)** The GO term of Top5 Pathway Ontology with -log10 (FDR *p*-value). **D)** Sequence coverage of identified tryptic fragment peptide from Alzheimer's disease-related protein (Tau, APP, SNCA, APOE) by LC-MS/MS analysis. Identified peptides are shown in black bold. Identified phosphorylation sites are indicated in red bold. **E)** KEGG pathway of Alzheimer Disease. The 68 proteins identified in the AD group are highlighted by red stars.

Figure 3. Label-free quantitative proteomics comparison of AD brain-derived EVs and CTRL brain-derived EVs:

A) Venn diagram representing the number of EV proteins differentially expressed in CTRL and AD. **B)** The quantitative proteome profiles obtained by the label-free analysis were used to inform a principal components analysis (PCA). CTRL samples are defined by blue symbols, AD samples by red symbols. **C)** Volcano plot showing a degree of differential expression of EV proteins in AD compared with CTRL. The x-axis indicates log transformed fold change in expression. The y-axis shows log-transformed *p*-values. The grey dot line shows the 0.1 *p*-values and 1 or -1 fold change cutoff. **D)** Heat map representation of the up- and down-regulated proteins in AD. Red shows up-regulated proteins, and Green shows down-regulated proteins. **E)** Enrichment of brain cell type-specific markers in brain-derived EV proteins. Yellow: Neuron, Purple: Microglia, Green: Astrocytes, Orange: Oligodendrocytes. The parentheses show the number and percentage of identified cell type-specific protein. **F)** Comparison of the cell type-

specific protein in AD brain-derived EV and CTRL EV. The red bar shows higher expression in AD. Blue bar indicates higher expression in CTRL.

Figure 4. Machine learning model to identify AD brain-specific EV biomarker molecules: **A)** Workflow for Machine learning approach. The training set is fed into LDA to generate LDA vectors, which are applied to the blinded test set for classification. The predicted molecule are then validated from the validation cohort by a commercial ELISA assay. **B)** The best performing panel based on the area under the ROC curve using the Lasso algorithm was selected in the training set. The y-axis shows the area under the ROC curve. The x-axis indicates the number of proteins selected by the Lasso algorithm in the training set. The green box shows the selected protein with High AUC for the blinded test set. **C)** The Accuracy for 4 proteins with high AUC chose to generate the label of the test set, and note on their outcome to generate the prediction on the test set. Randomly selected control: Accuracy = 55%, AUC = 0.58., Shuffling control: Accuracy = 47.6%, AUC=0.47. **D)** A scatter plot of log2 (normalized ratio) as measured by proteomics per selected candidate protein in Machine Learning. (ANXA5: p = 4.58E-06, log2 fold change = 1.1, VGF: p = 5.30E-04, log2 fold change = -1.6, GPM6A: p = 5.37E-04, log2 fold change = 0.6, ACTZ: p = 4.44E-03, log2 fold change = -1.5). **E)** Scattered plot of candidate molecules and AD pathogenic molecule in brain-derived EVs. Left: GPM6A and pS396 tau (r = 0.380, p = 0.019). Center: GPM6A and Aβ1-42 (r = 0.387, p = 0.016). Right: VGF and Aβ1-42 (r = -0.538, p = 0.002). **F)** Left: ELISA revealed that there is significant difference in total ANXA5 to total EV protein between AD and CTRL group (p = 0.0042 by Mann-Whitney test) (AD = 42, CTRL = 36). Right: Braak stage-dependent increase in the ANXA5 expression level to total EV protein in AD dependent manner.

Table 1. Patients information

Discovery set

For proteomics	AD (n=20)	Control (n=18)	*p*-value[a]
Age, mean	75.0 ± 9.12	75.7 ± 8.88	0.997
Gender (male, female)	15M, 5F	14M, 4F	
PMI, mean	12.5 ± 8.68	17.8 ± 7.57	0.0675

Validation set

For proteomics	AD (n=42)	Control (n=36)	*p*-value
Age, mean	81.0 ± 11.64	79.0 ± 11.59	0.1533
Gender (male, female)	24M, 17F	22M, 15F	
PMI, mean	9.0 ± 7.25	17.3 ± 8.28	0.0069

[a] The statistical significance of the differences were calculated using Mann-Whitney test.

Table 2. Up- and down- regulated protein in expression between AD and CTRL

UniProt ID	Protein name	log2 (Fold Change) (AD/ CTRL)[a]	-log10 (*p*-value)[a]
P08758	ANXA5	1.1	5.34
P17302	CXA1	1.0	3.54
Q9NRQ2	PLS4	1.4	3.11
P04083	ANXA1	1.0	3.10
Q9Y617	SERC	1.5	2.83
P61769	B2MG	1.0	2.55
Q15599	NHRF2	1.3	2.27
Q9BW30	TPPP3	1.0	2.18
P17931	LEG3	1.4	2.00
P31040	SDHA	1.1	1.90
P02792	FRIL	1.0	1.67
P00918	CAH2	1.1	1.55
Q9UH03	SEPT3	1.4	1.42
Q9Y6C9	MTCH2	1.7	1.33
Q13449	LSAMP	1.0	1.30
O15240	VGF	-1.6	3.28
Q9NR46	SHLB2	-1.3	1.67
O75061	AUXI	-1.0	2.00

[a]The log2 fold change were calculated by the protein intensity which was analyzed by PEAKS software.
[b]The statistical significance of the differences were calculated using Student's t test.

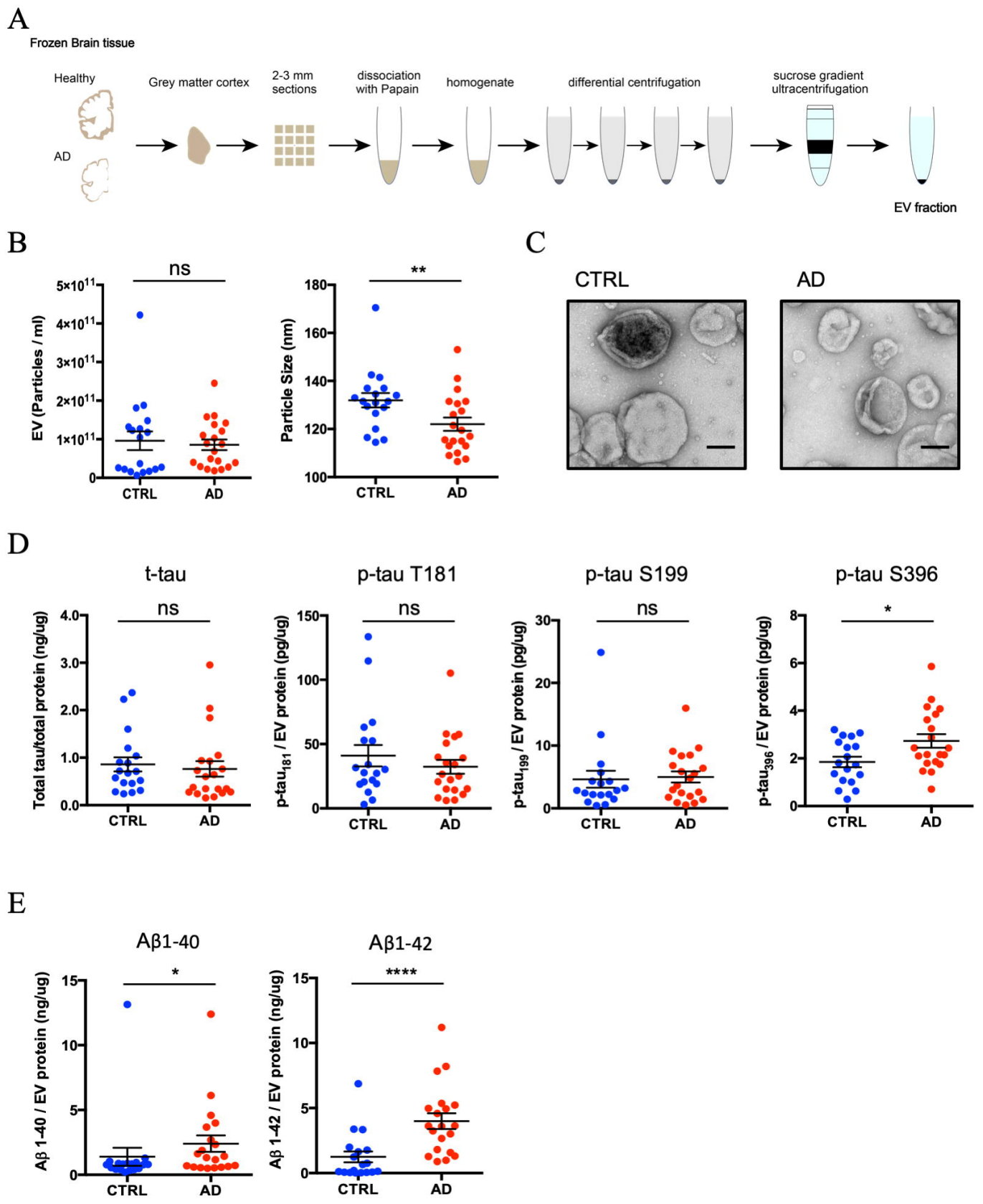
A
Frozen Brain tissue
Healthy
AD
Grey matter cortex
2-3 mm sections
dissociation with Papain
homogenate
differential centrifugation
sucrose gradient ultracentrifugation
EV fraction
B
ns
**
EV (Particles / ml)
Particle Size (nm)
CTRL
AD
C
CTRL
AD
D
t-tau
p-tau T181
p-tau S199
p-tau S396
Total tau/total protein (ng/ug)
p-tau181 / EV protein (pg/ug)
p-tau199 / EV protein (pg/ug)
p-tau396 / EV protein (pg/ug)
E
Aβ1-40
Aβ1-42
Aβ 1-40 / EV protein (ng/ug)
Aβ 1-42 / EV protein (ng/ug)

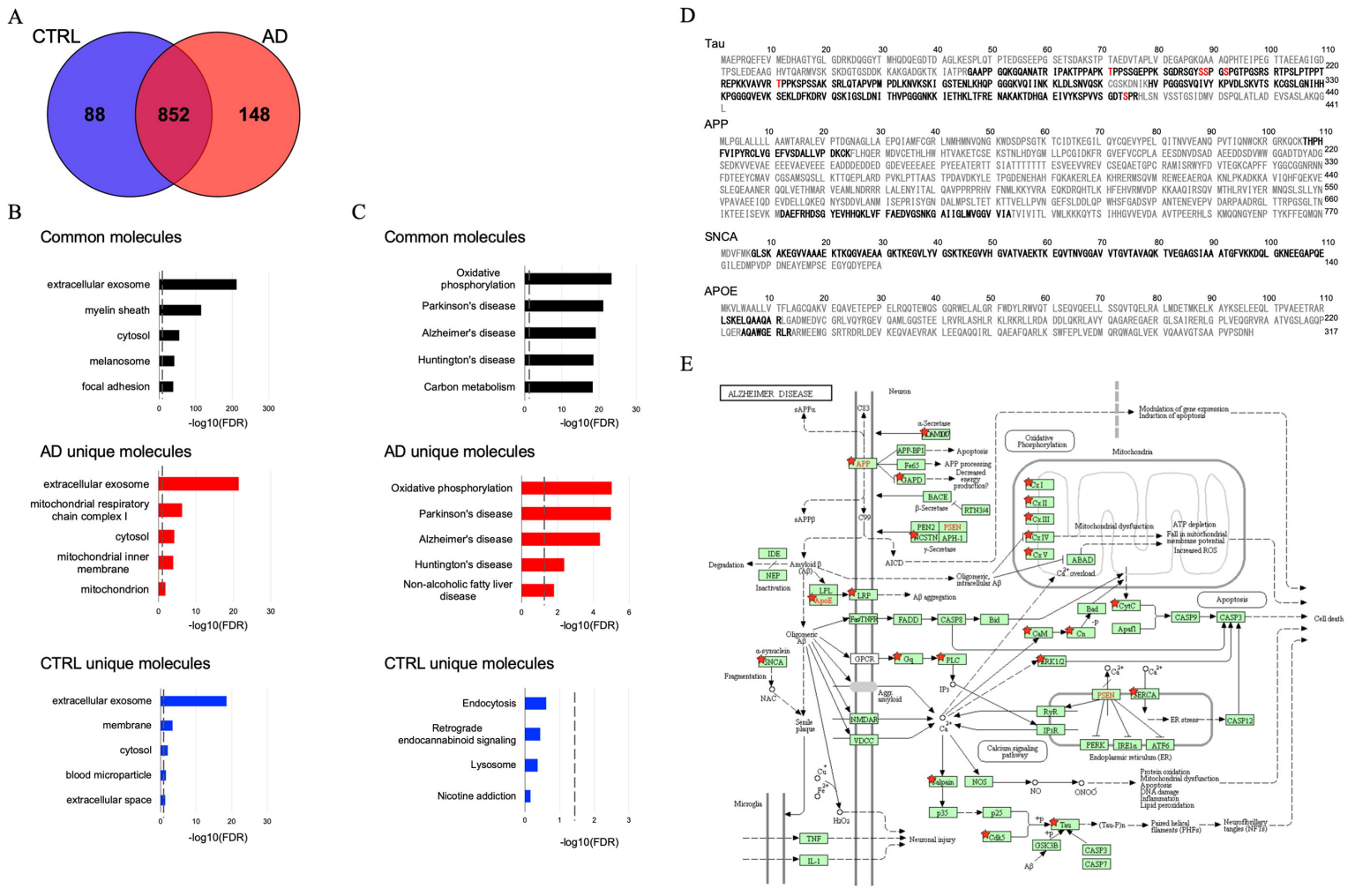
A
CTRL
AD
88
852
148
B
Common molecules
extracellular exosome
myelin sheath
cytosol
melanosome
focal adhesion
0
100
200
300
-log10(FDR)
AD unique molecules
extracellular exosome
mitochondrial respiratory chain complex I
cytosol
mitochondrial inner membrane
mitochondrion
0
10
20
30
-log10(FDR)
CTRL unique molecules
extracellular exosome
membrane
cytosol
blood microparticle
extracellular space
0
10
20
30
-log10(FDR)
C
Common molecules
Oxidative phosphorylation
Parkinson's disease
Alzheimer's disease
Huntington's disease
Carbon metabolism
0
10
20
30
-log10(FDR)
AD unique molecules
Oxidative phosphorylation
Parkinson's disease
Alzheimer's disease
Huntington's disease
Non-alcoholic fatty liver disease
0
2
4
6
-log10(FDR)
CTRL unique molecules
Endocytosis
Retrograde endocannabinoid signaling
Lysosome
Nicotine addiction
0
1
2
3
-log10(FDR)
D
Tau
10 20 30 40 50 60 70 80 90 100 110
MAEPRQEFEV MEDHAGTYGL GDRKDQGGYT MHQDQEGDTD AGLKESPLQT PTEDGSEEPG SETSDAKSTP TAEDVTAPLV DEGAPGKQAA AQPHTEIPEG TTAEEAGIGD
TPSLEDEAAG HVTQARMVSK SKDGTGSDDK KAKGADGKTK IATPRGAAPP GQKGQANATR IPAKTPPAPK TPPSSGEPPK SGDRSGYSSP GSPGTPGSRS RTPSLPTPPT
REPKKVAVVR TPPKSPSSAK SRLQTAPVPM PDLKNVKSKI GSTENLKHQP GGGKVQIINK KLDLSNVQSK CGSKDNIKHV PGGGSVQIVY KPVDLSKVTS KCGSLGNIHH
KPGGGQVEVK SEKLDFKDRV QSKIGSLDNI THVPGGGNKK IETHKLTFRE NAKAKTDHGA EIVYKSPVVS GDTSPRHLSN VSSTGSIDMV DSPQLATLAD EVSASLAKQG
L
APP
10 20 30 40 50 60 70 80 90 100 110
MLPGLALLLL AAWTARALEV PTDGNAGLLA EPQIAMFCGR LNMHMNVQNG KWDSDPSGTK TCIDTKEGIL QYCQEVYPEL QITNVVEANQ PVTIQNWCKR GRKQCKTHPH
FVIPYRCLVG EFVSDALLVP DKCKFLHQER MDVCETHLHW HTVAKETCSE KSTNLHDYGM LLPCGIDKFR GVEFVCCPLA EESDNVDSAD AEEDDSDVWW GGADTDYADG
SEDKVVEVAE EEEVAEVEEE EADDDEDDED GDEVEEEAEE PYEEATERTT SIATTTTTTT ESVEEVVREV CSEQAETGPC RAMISRWYFD VTEGKCAPFF YGGCGGNRNN
FDTEEYCMAV CGSAMSQSLL KTTQEPLARD PVKLPTTAAS TPDAVDKYLE TPGDENEHAH FQKAKERLEA KHRERMSQVM REWEEAERQA KNLPKADKKA VIQHFQEKVE
SLEQEAANER QQLVETHMAR VEAMLNDRRR LALENYITAL QAVPPRPRHV FNMLKKYVRA EQKDRQHTLK HFEHVRMVDP KKAAQIRSQV MTHLRVIYER MNQSLSLLYN
VPAVAEEIQD EVDELLQKEQ NYSDDVLANM ISEPRISYGN DALMPSLTET KTTVELLPVN GEFSLDDLQP WHSFGADSVP ANTENEVEPV DARPAADRGL TTRPGSGLTN
IKTEEISEVK MDAEFRHDSG YEVHHQKLVF FAEDVGSNKG AIIGLMVGGV VIATVIVITL VMLKKKQYTS IHHGVVEVDA AVTPEERHLS KMQQNGYENP TYKFFEQMQN
SNCA
10 20 30 40 50 60 70 80 90 100 110
MDVFMKGLSK AKEGVVAAAE KTKQGVAEAA GKTKEGVLYV GSKTKEGVVH GVATVAEKTK EQVTNVGGAV VTGVTAVAQK TVEGAGSIAA ATGFVKKDQL GKNEEGAPQE
GILEDMPVDP DNEAYEMPSE EGYQDYEPEA
140
APOE
10 20 30 40 50 60 70 80 90 100 110
MKVLWAALLV TFLAGCQAKV EQAVETEPEP ELRQQTEWQS GQRWELALGR FWDYLRWVQT LSEQVQEELL SSQVTQELRA LMDETMKELK AYKSELEEQL TPVAEETRAR
LSKELQAAQA RLGADMEDVC GRLVQYRGEV QAMLGQSTEE LRVRLASHLR KLRKRLLRDA DDLQKRLAVY QAGAREGAER GLSAIRERLG PLVEQGRVRA ATVGSLAGQP
LQERAQAWGE RLRARMEEMG SRTRDRLDEV KEQVAEVRAK LEEQAQQIRL QAEAFQARLK SWFEPLVEDM QRQWAGLVEK VQAAVGTSAA PVPSDNH
317
E
ALZHEIMER DISEASE
Neuron
sAPPα
C83
α-Secretase
ADAM10
APP
APP-BP1
Fe65
JAPD
BACE
β-Secretase
RTN3i4
sAPPβ
C99
PEN2
PSEN
NCSTN
APH-1
γ-Secretase
AICD
IDE
Degradation
Amyloid β (Aβ)
NEP
Inactivation
LPL
ApoE
LRP
Aβ aggregation
Oligomeric intracellular Aβ
Oligomeric Aβ
α-synuclein
SNCA
Fragmentation
NAC
Senile plaque
Aggr. survival
NMDAR
VDCC
Ca2+
GPCR
Gq
PLC
IP3
ERK1/2
Modulation of gene expression
Induction of apoptosis
Oxidative Phosphorylation
Mitochondria
CxI
CxII
CxIII
CxIV
CxV
Mitochondrial dysfunction
ATP depletion
Fall in mitochondrial membrane potential
Increased ROS
ABAD
Ca2+ overload
Apoptosis
FasTNFR
FADD
CASP8
Bid
CytC
Apaf1
CASP9
CASP3
Cell death
CaM
Cn
P
PSEN
SERCA
RyR
IP3R
ER stress
CASP12
Calcium signaling pathway
PERK
IRE1α
ATF6
Endoplasmic reticulum (ER)
Calpain
NOS
NO
ONOO-
Protein oxidation
Mitochondrial dysfunction
Apoptosis
DNA damage
Inflammation
Lipid peroxidation
Microglia
H2O2
p35
p25
Cdk5
Tau
(Tau-P)n
Paired helical filaments (PHFs)
Neurofibrillary tangles (NFTs)
GSK3B
CASP3
CASP7
Aβ
TNF
IL-1
Neuronal injury

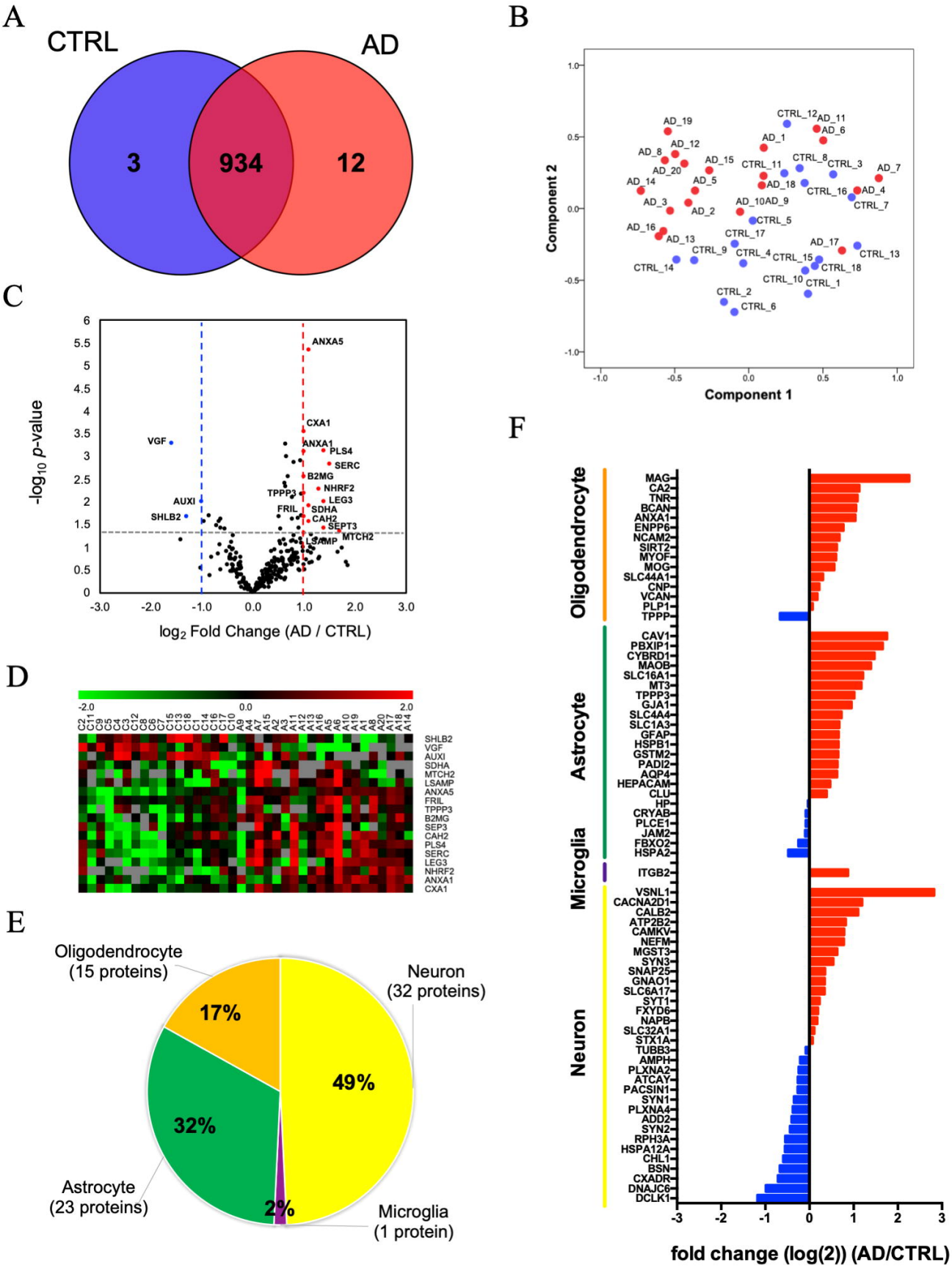
A
CTRL
AD
3
934
12
B
Component 2
Component 1
C
-log10 p-value
log2 Fold Change (AD / CTRL)
ANXA5
CXA1
VGF
ANXA1
PLS4
SERC
B2MG
NHRF2
TPPP3
LEG3
AUXI
FRIL
SDHA
SHLB2
CAH2
SEPT3
MTCH2
LSAMP
D
SHLB2
VGF
AUXI
SDHA
MTCH2
LSAMP
ANXA5
FRIL
TPPP3
B2MG
SEP3
CAH2
PLS4
SERC
LEG3
NHRF2
ANXA1
CXA1
E
Oligodendrocyte
(15 proteins)
17%
Neuron
(32 proteins)
49%
32%
Astrocyte
(23 proteins)
2%
Microglia
(1 protein)
F
Oligodendrocyte
Astrocyte
Microglia
Neuron
MAG
CA2
TNR
BCAN
ANXA1
ENPP6
NCAM2
SIRT2
MYOF
MOG
SLC44A1
CNP
VCAN
PLP1
TPPP
CAV1
PBXIP1
CYBRD1
MAOB
SLC16A1
MT3
TPPP3
GJA1
SLC4A4
SLC1A3
GFAP
HSPB1
GSTM2
PADI2
AQP4
HEPACAM
CLU
HP
CRYAB
PLCE1
JAM2
FBXO2
HSPA2
ITGB2
VSNL1
CACNA2D1
CALB2
ATP2B2
CAMKV
NEFM
MGST3
SYN3
SNAP25
GNAO1
SLC6A17
SYT1
FXYD6
NAPB
SLC32A1
STX1A
TUBB3
AMPH
PLXNA2
ATCAY
PACSIN1
SYN1
PLXNA4
ADD2
SYN2
RPH3A
HSPA12A
CHL1
BSN
CXADR
DNAJC6
DCLK1
fold change (log(2)) (AD/CTRL)

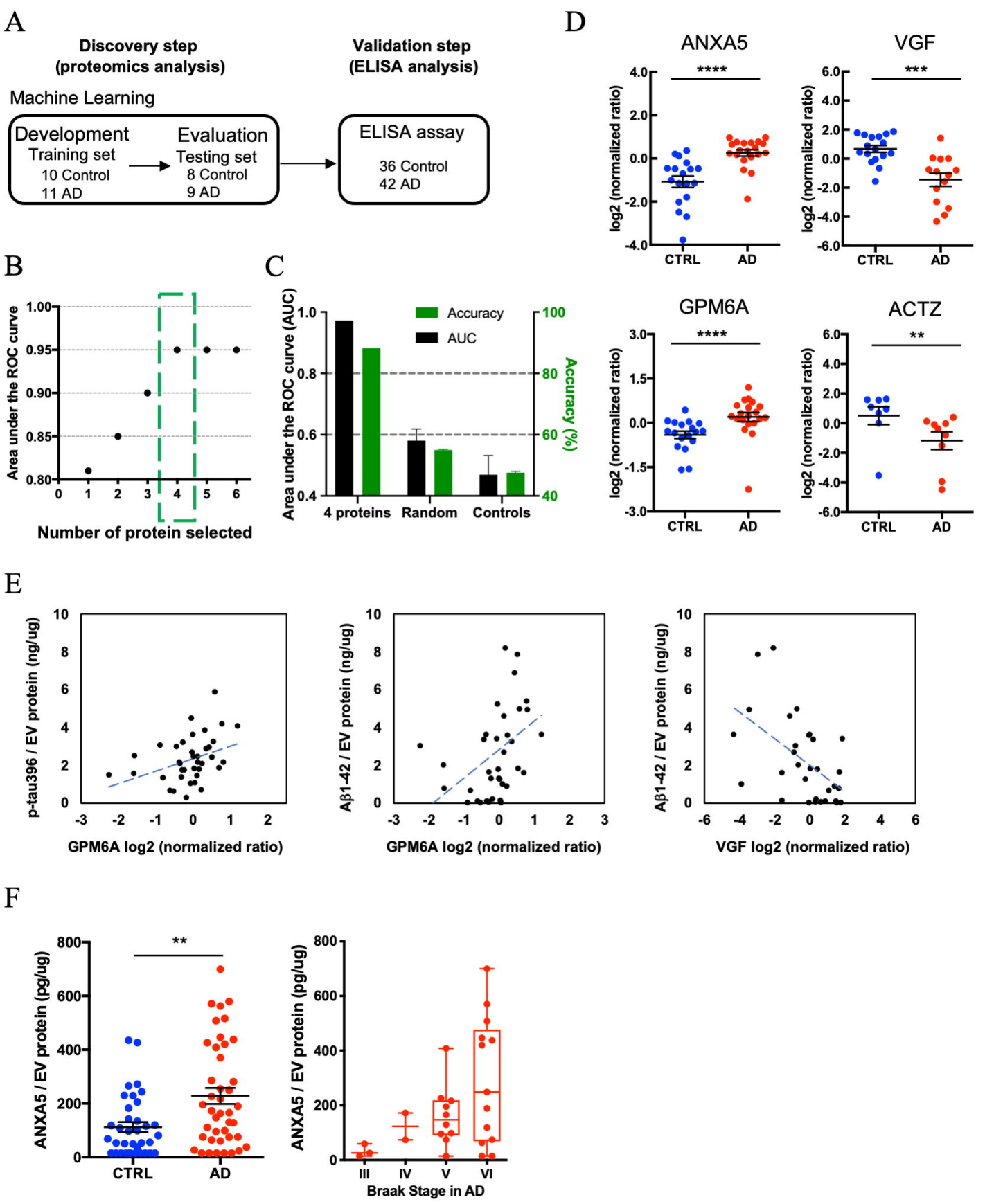
A
Discovery step
(proteomics analysis)
Validation step
(ELISA analysis)
Machine Learning
Development
Training set
10 Control
11 AD
Evaluation
Testing set
8 Control
9 AD
ELISA assay
36 Control
42 AD
B
Area under the ROC curve
Number of protein selected
C
Area under the ROC curve (AUC)
Accuracy
AUC
Accuracy (%)
4 proteins
Random
Controls
D
ANXA5
VGF
GPM6A
ACTZ
log2 (normalized ratio)
CTRL
AD
E
p-tau396 / EV protein (ng/ug)
GPM6A log2 (normalized ratio)
Aβ1-42 / EV protein (ng/ug)
VGF log2 (normalized ratio)
F
ANXA5 / EV protein (pg/ug)
Braak Stage in AD